



First- and second-order quantum phase transitions in the one-dimensional transverse-field Ising model with boundary fields

Kun Hu  and Xintian Wu**Department of Physics, Beijing Normal University, Beijing, 100875, China* (Received 20 July 2020; revised 20 December 2020; accepted 22 December 2020; published 8 January 2021)

The one-dimensional transverse field Ising model with boundary fields is studied analytically and numerically. The phase diagram in the ordered state is obtained. We find that there exist two types of phase transitions. The longitudinal boundary fields applied to the left and right ends of the Ising chain are h_L and h_R , respectively. For $|h_L|, |h_R| < \sqrt{1-g}$, where g is the transverse field and $h_L h_R < 0$, a first-order phase transition occurs with the changing h_L or h_R . The energy gap and boundary magnetization are solved exactly. The analytical expressions of the finite-size scaling for the first-order phase transition are obtained. For $|h_R| > \sqrt{1-g}$ and $h_L h_R < 0$, there exists a continuous phase transition with changing h_L and vice versa. This transition is identified as a quantum wetting transition. The singularity of the boundary magnetization in this phase transition is explicitly shown. A simple computational procedure with high accuracy and efficiency is proposed to calculate the magnetization. The magnetization profile, correlation functions, and wetting layer thickness are studied numerically.

DOI: [10.1103/PhysRevB.103.024409](https://doi.org/10.1103/PhysRevB.103.024409)

I. INTRODUCTION

Quantum phase transitions have attracted great interest in recent decades, driven by the experiments on various new materials, especially on topological materials in condensed matter and novel quantum systems provided by cold atoms [1–4]. The quantum Ising chain in a transverse field is a paradigmatic quantum many-body system that shows continuous and first-order quantum transitions [5]. This topic has been investigated in a vast number of studies [6–10]. Currently, it is still used as a testing field of new physics concepts [11] and closely related to the Kitaev model with topological order [12,13]. The cold atomic system can realize this model experimentally [4]. Furthermore, it can be mapped to the two-dimensional Ising model [1,14], which is the most important model in statistical physics and is now well understood [15–19].

However, some important and interesting phenomena are still poorly understood in this model. For the transverse field $g < 1$, the system is in an ordered state. If the boundary fields are applied, as shown in Fig. 1(a), quantum phase transitions occur as we change the boundary fields h_L, h_R . The red solid line representing $-\sqrt{1-g} < h_R = -h_L < \sqrt{1-g}$ in Fig. 1(b) is the border between the phases “Positive” and “Negative.” The phase transition between these two states is a first-order transition. The blue solid lines in Fig. 1(b) represent $|h_L| > \sqrt{1-g}$, $|h_R| = \sqrt{1-g}$ or $|h_R| > \sqrt{1-g}$, $|h_L| = \sqrt{1-g}$ and $h_L h_R < 0$. Across these borders, a second-order phase transition takes place.

The discontinuity in the first-order phase transition is shown in Fig. 1(c). The boundary magnetization (of the left first spin) shows a jump as we fix h_R and change h_L . In

particular, for $h_R \rightarrow 0$ [red dashed curve in Fig. 1(c)], the boundary magnetization at the equilibrium state jumps from negative to positive as h_L changes from negative to positive. The finite-size scaling (FSS) for the energy gap and the boundary magnetization are solved exactly. Figure 1(d) shows the boundary magnetization versus h_L for the second-order phase transition, which has a cusp. The discontinuity in the derivative of the boundary magnetization is obtained rigorously. In addition, we propose a simple computational procedure to compute the correlation functions and magnetization with high accuracy and efficiency. This procedure can be carried out on very large lattice sizes of up to $N = 6400$. Figures 1(c) and 1(d) show the numerical results obtained with this computational procedure.

It is well known that the one-dimensional quantum spin model can be mapped to the 1+1 dimensional classical spin model [14]. In other words, the one-dimensional transverse field Ising model is the quantum version of the two-dimensional Ising model, which is understood thoroughly [16,18]. There exists a wetting transition in the two-dimensional Ising model with surface fields. The exact solution of the wetting transition was obtained by Abraham 40 years ago [20,21], which is called the Abraham model. On the other hand, the one-dimensional transverse Ising model was solved earlier in 1970 by Pfeuty [5]. Interestingly, the wetting transition in the transverse field Ising model has not been studied until recently. Campostrini *et al.* studied the transverse field Ising model with boundary fields several years ago [22]. These authors pointed out that a wetting transition exists. In their work, the boundary fields are antisymmetric for the wetting transition. These boundary fields are not suitable to study some important properties of the wetting transition such as the wetting layer thickness. Moreover, their work focused on the finite-size scaling of the energy gap and correlation functions rather than the wetting transition, and

*Corresponding author: wuxt@bnu.edu.cn

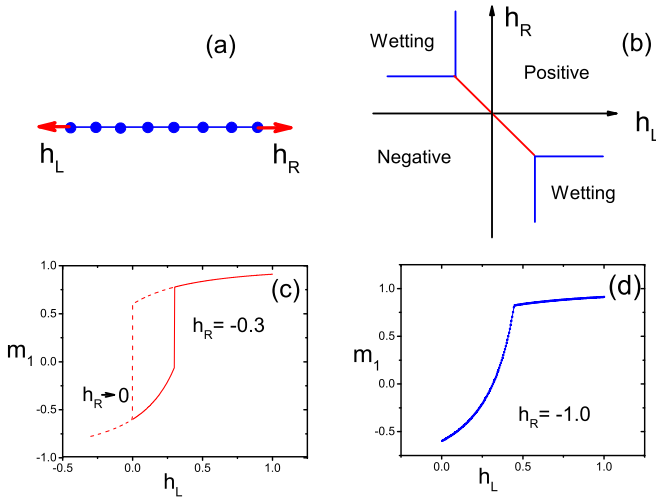


FIG. 1. (a) Sketch of the model with surface fields. (b) Phase diagram. (c) First-order phase transition across the border represented by the red line in panel (b) with $g = 0.8$. (d) Continuous phase transition across the border represented by the blue lines in panel (b) with $g = 0.8$.

the detailed critical behavior of the wetting transition was not investigated. The second-order phase transition discussed in this work is identified as a quantum wetting transition. We compare the classical and quantum wetting transitions in detail.

Because the basic reasoning for the one-dimensional transverse field Ising model with boundary fields has already been described in detail in the literature [22], we clearly state the contribution of the present study. First, we solved the eigenvectors in the exact diagonalization technique and computed the boundary magnetization semianalytically. Second, we obtained the exact finite-size scaling of the boundary magnetization for the first-order phase transition. Third, we studied the wetting layer thickness in detail due to the presence of opposite boundary fields with different strengths. This information includes the finite-size scaling behavior of the boundary magnetization, the magnetization profile and the order-parameter correlation length.

The rest of the paper is arranged as follows. In Sec. II we introduce the transverse field Ising model with boundary fields. In Sec. III we solve the eigenvectors for the Bogoliubov transformation. In Sec. IV we study the first-order phase transition between the “Positive” and “Negative” phases. In Sec. V we discuss the second-order phase transition, i.e., the quantum wetting transition. Section VI summarizes this work.

II. HAMILTONIAN DIAGONALIZATION AND FORMULATION OF MAGNETIZATION

A. Jordan-Wigner transformation and Bogoliubov transformation

We consider the one-dimensional transverse field Ising chain with boundary fields:

$$H = H_0 - h_L \sigma_1^{(1)} - h_R \sigma_N^{(1)}, \quad (1)$$

where

$$H_0 = - \sum_{i=1}^{i=N-1} K_i \sigma_i^{(1)} \sigma_{i+1}^{(1)} - g \sum_{i=1}^{i=N} \sigma_i^{(3)}; \quad (2)$$

here $\sigma_i^{(1)}, \sigma_i^{(3)}$ are Pauli matrices, K_i are the couplings, and h_L, h_R are the left and right boundary longitudinal fields, respectively. Following the well-known theories [22–25], we transform the diagonalization problem to an effective Hamiltonian by appending one additional spin to the left and right sides. The corresponding Hamiltonian is given by

$$H_e = H_0 - |h_L| \sigma_0^{(1)} \sigma_1^{(1)} - |h_R| \sigma_N^{(1)} \sigma_{N+1}^{(1)}. \quad (3)$$

Because $\sigma_0^{(1)}, \sigma_{N+1}^{(1)}$ are free from the transverse field, both $\sigma_0^{(1)}, \sigma_{N+1}^{(1)}$ commute with the Hamiltonian. Hence, they can be diagonalized simultaneously. The Hilbert space can be divided into four sectors, which we label $(1, 1), (1, -1), (-1, 1), (-1, -1)$, where (s_0, s_{N+1}) are eigenvalues of $\sigma_0^{(1)}$ and $\sigma_{N+1}^{(1)}$. The restriction of H_e to the four sectors gives rise to the Hamiltonian H with four cases of different signs of h_L, h_R [22]. For example, the restriction of H_e to sector $(1, -1)$ gives rise to the Hamiltonian H with $h_L > 0, h_R < 0$. The first- and second-order phase transitions occur at the region $h_L h_R < 0$. Therefore, we investigate the case $h_L > 0, h_R < 0$ and the sector $(1, -1)$. The case $h_L < 0, h_R > 0$ can be obtained with symmetry.

To compute the spectrum of the Hamiltonian (3), we perform the Jordan-Wigner transformation and define fermionic operators

$$c_i^\dagger = (-1)^j \prod_{j=0}^{i-1} \sigma_j^{(3)} \sigma_i^+, \quad (4)$$

where $\sigma^\pm = (\sigma^{(1)} \pm i\sigma^{(2)})/2$ (i is the imaginary unit). The Hamiltonian becomes

$$H_e = -gN + \sum_{i,j=0}^{N+1} \left(c_i^\dagger \mathbf{A}_{ij} c_j + \frac{1}{2} c_i^\dagger \mathbf{B}_{ij} c_j^\dagger - \frac{1}{2} c_i \mathbf{B}_{ij} c_j \right), \quad (5)$$

where \mathbf{A} and \mathbf{B} are symmetric and antisymmetric matrices, respectively. For clarity here we write the matrix elements explicitly for $N = 3$ in the following:

$$\mathbf{A} = \begin{pmatrix} 0 & -|h_L| & 0 & 0 & 0 \\ -|h_L| & -2g & -K_1 & 0 & 0 \\ 0 & -K_1 & -2g & -K_2 & 0 \\ 0 & 0 & -K_2 & -2g & -|h_R| \\ 0 & 0 & 0 & -|h_R| & 0 \end{pmatrix}, \quad (6)$$

$$\mathbf{B} = \begin{pmatrix} 0 & -|h_L| & 0 & 0 & 0 \\ |h_L| & 0 & -K_1 & 0 & 0 \\ 0 & K_1 & 0 & -K_2 & 0 \\ 0 & 0 & K_2 & 0 & -|h_R| \\ 0 & 0 & 0 & |h_R| & 0 \end{pmatrix}. \quad (7)$$

We perform a Bogoliubov transformation by introducing new canonical fermionic variables [26]

$$\eta_k = g_{k,i} c_i + h_{k,i} c_i^\dagger. \quad (8)$$

Using these variables, the Hamiltonian can be diagonalized. The coefficients $g_{k,i}$, $h_{k,i}$ satisfy the following equations:

$$g_{ki} = \frac{\phi_{k,i} + \psi_{k,i}}{2}, \quad h_{ki} = \frac{\phi_{k,i} - \psi_{k,i}}{2}, \quad (9)$$

where ψ_k is the eigenvector of the matrix

$$\mathbf{C} \equiv (\mathbf{A} + \mathbf{B})(\mathbf{A} - \mathbf{B}), \quad \mathbf{C}\psi_k = \varepsilon_k^2 \psi_k \quad (10)$$

and

$$\phi_k = (\mathbf{A} - \mathbf{B})\psi_k / \varepsilon_k. \quad (11)$$

In the above equation, $\varepsilon_k \neq 0$. There is a zero eigenvalue $\varepsilon_0 = 0$ for \mathbf{C} , and this mode is treated in Ref. [22]. For the convenience of the readers, we write the matrix \mathbf{C} 's elements explicitly for $N = 3$:

$$\mathbf{C} = 4 \begin{pmatrix} h_L^2 & g|h_L| & 0 & 0 & 0 \\ g|h_L| & K_1^2 + g^2 & gK_1 & 0 & 0 \\ 0 & gK_1 & K_2^2 + g^2 & gK_2 & 0 \\ 0 & 0 & gK_2 & |h_R|^2 + g^2 & 0 \\ 0 & 0 & 0 & 0 & 0 \end{pmatrix}. \quad (12)$$

It is clear that there is a zero eigenvalue $\varepsilon_0 = 0$ for \mathbf{C} . The spectrum is doubly degenerate due to this zero mode. This degeneracy is the consequence of the Z_2 global symmetry of the Hamiltonian H_e . The zero mode is not related to the spectrum of the Hamiltonian H . Only the nonzero modes are relevant. There are $N + 1$ nonzero modes that we label by $k = 1, 2, \dots, N + 1$. Here $0 = \varepsilon_0 < \varepsilon_1 < \varepsilon_2 \dots$.

Generally, the couplings K_i can be arbitrary. In this work, we consider only the uniform couplings, $K_i = 1$.

B. Energy gap and magnetization for opposite boundary fields

The two degenerate ground states for the Hamiltonian H_e belong to the sectors $(-1, -1)$ and $(1, 1)$ [22]. Here we consider the ground state of H_e belonging to the sector $(-1, -1)$, described by

$$\sigma_0^{(1)}|\Psi_0\rangle = \sigma_{N+1}^{(1)}|\Psi_0\rangle = -|\Psi_0\rangle. \quad (13)$$

For the Hamiltonian H with $h_L > 0$, $h_R < 0$, the ground state and the first excited state are the first and second excited states of H_e , respectively. They belong to sector $(1, -1)$ and are given by

$$|\Psi_1\rangle = \eta_1^\dagger|\Psi_0\rangle, \quad |\Psi_2\rangle = \eta_2^\dagger|\Psi_0\rangle. \quad (14)$$

The energy gap is given by the difference between the energies of these two states:

$$\Delta = \varepsilon_2 - \varepsilon_1. \quad (15)$$

Why do $|\Psi_1\rangle, |\Psi_2\rangle$ belong to sector $(1, -1)$? Since it is shown that [22]

$$\{\sigma_0^{(1)}, \eta_k\} = [\sigma_{N+1}^{(1)}, \eta_k] = 0, \quad (16)$$

we have

$$\sigma_0^{(1)}|\Psi_1\rangle = \sigma_0^{(1)}\eta_1^\dagger|\Psi_0\rangle = -\eta_1^\dagger\sigma_0^{(1)}|\Psi_0\rangle = |\Psi_1\rangle \quad (17)$$

and

$$\sigma_{N+1}^{(1)}|\Psi_1\rangle = -|\Psi_1\rangle. \quad (18)$$

That is, $\eta_k^\dagger|\Psi_0\rangle$ belongs to sector $(1, -1)$. As mentioned above, the restriction of H_e to sector $(1, -1)$ gives rise to the Hamiltonian with boundary fields H . Therefore, $\eta_1^\dagger|\Psi_0\rangle, \eta_2^\dagger|\Psi_0\rangle$ are the ground and first excited states of H , respectively.

To calculate the correlation function, we need to know the basic properties of the ground state $|\Psi_1\rangle$ for the Hamiltonian H with $h_L > 0$, $h_R < 0$. From Eq. (14), it is observed that

$$\eta_1^\dagger\eta_1|\Psi_1\rangle = |\Psi_1\rangle, \quad \eta_1\eta_1^\dagger|\Psi_1\rangle = 0 \quad (19)$$

and

$$\eta_j^\dagger\eta_j|\Psi_1\rangle = 0, \quad \eta_j\eta_j^\dagger|\Psi_1\rangle = |\Psi_1\rangle, \quad j > 1. \quad (20)$$

We define two operators:

$$B_i = c_i^\dagger - c_i, \quad A_i = c_i^\dagger + c_i. \quad (21)$$

From Ref. [26]

$$B_i = \sum_{k=1}^{N+1} (\eta_k^\dagger - \eta_k)\psi_{k,i} \quad (22)$$

and

$$A_i = \sum_{k=1}^{N+1} (\eta_k^\dagger + \eta_k)\phi_{k,i}. \quad (23)$$

In light of Eqs. (19) and (20), we obtain the contraction

$$G_{i,j} = \langle \Psi_1 | B_i A_j | \Psi_1 \rangle = \psi_{1,i} \phi_{1,j} - \sum_{k=2}^{N+1} \psi_{k,i} \phi_{k,j}. \quad (24)$$

These contractions are used in the calculations of the correlation functions. Following Ref. [26], we obtain the correlation function

$$\begin{aligned} & \langle \Psi_1 | \sigma_i^{(1)} \sigma_j^{(1)} | \Psi_1 \rangle \\ &= \langle \Psi_1 | B_i A_{i+1} B_{i+1} \cdots A_{j-1} B_{j-1} A_j | \Psi_1 \rangle \\ &= \begin{bmatrix} G_{i,i+1} & G_{i,i+2} & \cdots & G_{i,j} \\ G_{i+1,i+1} & G_{i+1,i+2} & \cdots & G_{i+1,j} \\ \cdots & \cdots & \cdots & \cdots \\ G_{j-1,i+1} & G_{j-1,i+2} & \cdots & G_{j-1,j} \end{bmatrix}, \end{aligned} \quad (25)$$

where $j > i$.

Since $\sigma_0^{(1)}$ commutes with the Hamiltonian H_e , the magnetization of the j th spin is related to the correlation function given by

$$m_j = \langle \Psi_1 | \sigma_j^{(1)} | \Psi_1 \rangle = \frac{1}{s_0} \langle \Psi_1 | \sigma_0^{(1)} \sigma_j^{(1)} | \Psi_1 \rangle, \quad (26)$$

where s_0 is the eigenvalue of $\sigma_0^{(1)}$. Based on the above equation, we propose an efficient computational procedure to calculate the magnetization. In the numerical calculation, we diagonalize the matrix \mathbf{C} using LAPACK and then obtain ψ_k, ϕ_k . We calculate the contraction $B_i A_j$ with Eq. (24). Then we can obtain the magnetization of j th spin with Eq. (26). The plots of the magnetization profile in the figures are the numerical results of this computational procedure.

The boundary magnetization of σ_1 can be investigated analytically. Since $\sigma_0^{(1)}\sigma_1^{(1)} = B_0 A_1$, from Eqs. (26), (24), and

(11), we obtain

$$m_1 = \frac{1}{2h_L s_0} \left[-\varepsilon_1 \psi_{1,0}^2 + \sum_{k=2}^{N+1} \varepsilon_k \psi_{k,0}^2 \right]. \quad (27)$$

C. Energy gap and magnetization for parallel boundary fields

Although we mainly study the case with opposite boundary fields, we present the method for the parallel boundary fields. In these cases, the ground state of H is the ground state of H_e . The ground state for the Hamiltonian H_e belonging to sector (1,1) is the ground state of H with $h_L > 0, h_R > 0$ [22]. For the ground state of H_e belonging to sector (1,1), we have

$$\sigma_0^{(1)} |\Psi_0\rangle = \sigma_{N+1}^{(1)} |\Psi_0\rangle = |\Psi_0\rangle. \quad (28)$$

For the Hamiltonian H , the first excited state is merely the first excited state of H_e . It is given by

$$|\Psi_1\rangle = \eta_1^\dagger |\Psi_0\rangle. \quad (29)$$

The energy gap is given by the difference between the energies of these two states:

$$\Delta = \varepsilon_1. \quad (30)$$

This leads to the contraction

$$G_{i,j} = \langle \Psi_1 | B_i A_j | \Psi_1 \rangle = - \sum_{k=1}^{N+1} \psi_{k,i} \phi_{k,j}. \quad (31)$$

Substituting these contractions into Eq. (25), we obtain the correlation function [26]. Then we obtain the magnetization with Eq. (26). The boundary magnetization of σ_1 becomes

$$m_1 = \frac{1}{2h_L s_0} \left[\sum_{k=1}^{N+1} \varepsilon_k \psi_{k,0}^2 \right]. \quad (32)$$

Therefore, we can calculate the energy gap and magnetization and the correlation function for all cases of h_L, h_R with different signs.

III. EIGENVECTORS OF MATRIX C

There are two types of eigenvectors for the matrix C : extended states and localized states. The extended states can be solved by assuming

$$\psi_{n,0} = \frac{c}{h_L} \sin \gamma_L, \quad \psi_{n,j} = (-1)^j c \sin(jk_n + \gamma_L), \quad (33)$$

where $j = 1, 2, \dots, N$ and the eigenvalue is given by

$$\varepsilon_n^2 = 1 + g^2 - 2g \cos k_n. \quad (34)$$

The phase shift γ_L and the wave vector k_n are determined by the boundary conditions. At the left boundary, we obtain

$$\frac{\sin(k_n + \gamma_L)}{\sin \gamma_L} = \frac{(h_L^2 - \varepsilon_n^2)}{gh_L^2}. \quad (35)$$

Some calculation leads to

$$\cot \gamma_L = a \tan \frac{k_n}{2} + \frac{b}{\sin k_n}, \quad (36)$$

where

$$a = 1 - \frac{2}{h_L^2}, \quad b = \frac{1-g}{g} \left(1 - \frac{1-g}{h_L^2} \right). \quad (37)$$

At the right boundary, we obtain

$$\frac{\sin[(N-1)k_n + \gamma_L]}{\sin(Nk_n + \gamma_L)} = \frac{(h_R^2 - 1 + 2g \cos k_n)}{g}. \quad (38)$$

Letting $k_n N + \gamma_L = n\pi - \gamma_R$, we obtain

$$\frac{\sin(k_n + \gamma_R)}{\sin \gamma_R} = \frac{(h_R^2 - 1 + 2g \cos k_n)}{g}. \quad (39)$$

This leads to

$$\cot \gamma_R = \frac{1 - x_R}{\sin k_n} - \tan \left(\frac{k_n}{2} \right), \quad (40)$$

where $x_R = (1 - h_R^2)/g$. The wave vectors are given by

$$k_n = \frac{n\pi - \gamma_L - \gamma_R}{N}, \quad n = n_0 + 1, n_0 + 2, \dots, N, \quad (41)$$

where $n_0 = 2$ for $0 < h_L, -h_R < \sqrt{1-g}$; $n_0 = 1$ for $0 < h_L < \sqrt{1-g} < -h_R$; and $n_0 = 0$ for $\sqrt{1-g} < h_L, -h_R$. The reason is as follows. We set $0 \leq \gamma_L, \gamma_R \leq \pi$. For $b > 0$, we have $\gamma_L = 0$ for $k_n \rightarrow 0$, while for $b < 0$, we have $\gamma_L = \pi$ for $k_n \rightarrow 0$. It is observed that $b = 0$ is a singular point at which the phase shift jumps from 0 to π as b changes sign. The parameter b changes sign at $h_L = \sqrt{1-g}$. A similar conclusion is reached for the phase shift γ_R . Therefore, we obtain n_0 for the three cases.

For small N , the normalization constant has some dependence on the phase shift γ_L, γ_R . For $N, n \gg 1$, the normalization constant is given by

$$c = \sqrt{\frac{2}{N}}. \quad (42)$$

There exist localized state eigenvectors of matrix C . For an Ising chain with size N , these eigenvectors are given by

$$\begin{aligned} \psi_{k,0} &= (\alpha u + \beta v x^{-N})/h_L, \\ \psi_{k,j} &= (-1)^j (\alpha u x^{-j} + \beta v x^{j-N}), \end{aligned} \quad (43)$$

where $k = 1, 2$ label the possible eigenvectors and $1 \leq j \leq N$. The parameters α, β are defined by

$$\alpha = \frac{h_L \sqrt{x_L^2 - 1}}{\sqrt{x_L^2 + h_L^2 - 1}}, \quad \beta = \frac{\sqrt{x_R^2 - 1}}{x_R}, \quad (44)$$

where

$$x_{L,R} = \frac{1 - h_{L,R}^2}{g}. \quad (45)$$

The eigenvalues of these eigenvectors satisfy

$$\varepsilon^2 = 4[1 + g^2 - g(x + x^{-1})]. \quad (46)$$

Substituting into Eq. (10), we obtain

$$\begin{aligned} (x - x_L)u + \delta_L v &= 0, \\ \delta_R u + (x - x_R)v &= 0, \end{aligned} \quad (47)$$

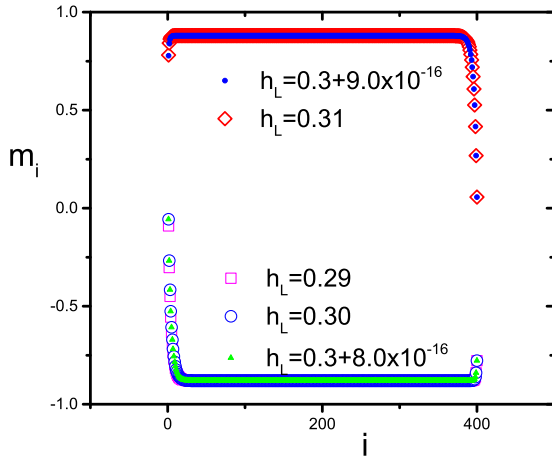


FIG. 2. Magnetization profiles around the first-order phase transition at $h_L = |h_R|$ with $h_R = -0.3$. The transverse field is set to be $g = 0.8$. The length of the chain is $N = 400$. The numerical calculation is carried out with double precision.

where

$$\delta_L = \frac{\beta}{\alpha} r (x^{-1} - x_L) x^{-N}, \quad \delta_R = \frac{\alpha}{\beta} (x^{-1} - x_R) x^{-N} \quad (48)$$

and

$$r = \frac{1 - gx}{1 - gx^{-1}}. \quad (49)$$

The real root of x requires that

$$x_L = \frac{1 - h_L^2}{g} > 1, \quad x_R = \frac{1 - h_R^2}{g} > 1. \quad (50)$$

For $|h_L|, |h_R| < \sqrt{1 - g}$, there are two real roots for x . In the limit of $N \rightarrow \infty$, we have $\delta_L, \delta_R \rightarrow 0$, and then, the two roots are given by $x_{L,R}$, corresponding to two states localized at the two boundaries, respectively. It turns out that α, β are the normalization constants for the two localized states. In the state localized at the left end, $u = 1, v = 0$, and in the state at the right end, $u = 0, v = 1$. It is observed from Eq. (46) that the energies of these states are given by

$$\varepsilon_{L,R} = 2\sqrt{1 + g^2 - g(x_{L,R} + x_{L,R}^{-1})}, \quad (51)$$

respectively. As we change h_L , the energies cross at $h_L = -h_R$. For $|h_L|, |h_R|$ less than $\sqrt{1 - g}$, there is one real root. For $|h_L|, |h_R| > \sqrt{1 - g}$, there is no real root. These cases correspond to $n_0 = 2, 1, 0$ in Eq. (41), respectively.

IV. FIRST-ORDER PHASE TRANSITION BETWEEN THE “POSITIVE” AND “NEGATIVE” PHASES

The first-order phase transition occurs at

$$h_L = -h_R \quad (52)$$

for $|h_L|, |h_R| < \sqrt{1 - g}$ and $h_L h_R < 0$. We show the dramatic change in the magnetization profile with $N = 400$ in Fig. 2. We fix $h_R = -0.3$ and change h_L . For $h_L = 0.29 < |h_R|$, the right boundary field dominates, and the magnetization of most spins are negative. We call this state the “Negative” phase. For

$h_L = 0.31 > |h_R|$, the left boundary field dominates, and the magnetization is positive for the majority of the spins. We call this state the “Positive” phase. In the infinite-volume limit, the phase transition occurs at $h_L = |h_R| = 0.3$. However, due to limit of the precision, the phase transition does not occur only at $h_L = 0.30$. Even for $h_L = 0.3 + 8.0 \times 10^{-16}$, the system still stays in the “Negative” phase. For $h_L = 0.3 + 9 \times 10^{-16}$, the system changes drastically to the “Positive” phase due to the dominance of the left boundary field. The physical picture is simple: for two opposite boundary fields, the field with larger absolute value dominates.

It should be noted that the magnetization profiles are the values at the equilibrium state. Their changes are not the real dynamic process, which is a fluctuation-induced process. Such a process can be studied with out-of-equilibrium dynamics [10]

The inversion of the magnetization occurs in a very small range of h_L for large N . In the limit of $N \rightarrow \infty$, this range approaches zero. For a chain with size N in the scaling region $|h_L - |h_R|| \ll |h_R|$, in Eq. (47), we have

$$\delta_L \approx \delta_R \approx \delta = \frac{h_R (x_R^{-1} - x_R)}{\sqrt{1 - gx_R^{-1}}} x_R^{-N}. \quad (53)$$

Since $x_R > 1$, δ decays exponentially with the system size N . In the case of $\delta \ll 1$, Eq. (47) yields two real roots:

$$x_{1,2} = \frac{1}{2} [(x_L + x_R) \pm \sqrt{(x_L - x_R)^2 + 4\delta^2}]. \quad (54)$$

Substituting them into Eq. (46) obtains the energies $\varepsilon_1, \varepsilon_2$ of the two lowest states:

$$\varepsilon_{1,2} = 2\sqrt{1 + g^2 - g(x_{1,2} + x_{1,2}^{-1})}. \quad (55)$$

From $\Delta = \varepsilon_2 - \varepsilon_1$, we obtain the scaling relation for the energy gap:

$$\Delta = \Delta_0 \sqrt{1 + \kappa^2}, \quad (56)$$

where

$$\Delta_0 = \frac{4g(1 - x_R^{-2})\delta}{\varepsilon_R}, \quad \kappa = \frac{|h_R|(h_L - |h_R|)}{g\delta}; \quad (57)$$

here κ is the scaling variable. We test this scaling relation with the numerical solution of eigenvalues. Figure 3(a) shows the energy gaps versus h_L for the lattice sizes $N = 40, 50, 60, 70$. The data collapse on the above scaling relation is shown in Fig. 3(b). This scaling relation is in agreement with the two lowest energy states ansatz for the first-order quantum phase transition proposed by Campostrini *et al.* [6]. Moreover, it is exactly solved in this model.

Now, we discuss the jump of boundary magnetization m_1 shown in Fig. 3(c). The jump is related to the two lowest eigenvectors. For the two real roots $x_{1,2}$, the corresponding u, v are given by

$$u_1 = \frac{1}{\sqrt{2(\kappa_1 + \kappa\sqrt{\kappa_1})}}, \quad v_1 = -\frac{\kappa + \sqrt{\kappa_1}}{\sqrt{2(\kappa_1 + \kappa\sqrt{\kappa_1})}} \quad (58)$$

and

$$u_2 = \frac{1}{\sqrt{2(\kappa_1 - \kappa\sqrt{\kappa_1})}}, \quad v_2 = -\frac{\kappa - \sqrt{\kappa_1}}{\sqrt{2(\kappa_1 - \kappa\sqrt{\kappa_1})}}, \quad (59)$$

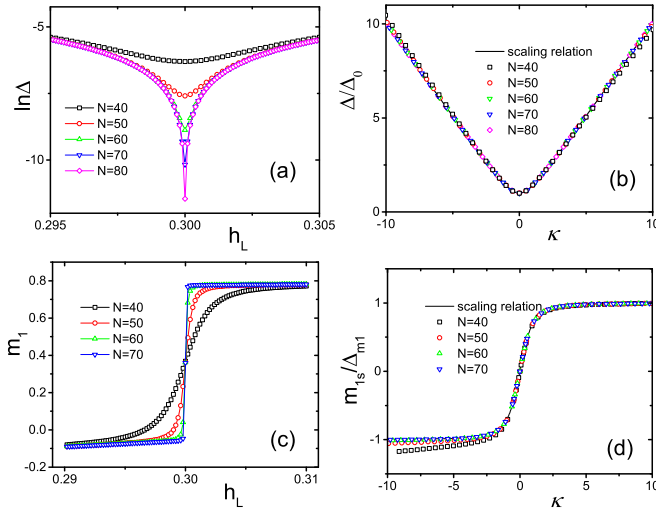


FIG. 3. (a) Numerical results for the energy gap for lattice sizes $N = 40, 50, 60, 70$ with $h_R = -0.3$. (b) Rescaled energy gaps approach the scaling relation Eq. (56). (c) The jumps of the boundary magnetization m_1 around the transition point. (d) The rescaled singular parts of boundary magnetization m_{1s} approach the scaling relation (62). In all cases, the transverse field is set to be $g = 0.8$.

where $\kappa_1 = 1 + \kappa^2$. Substitution into Eq. (43) leads to the eigenvectors of the two lowest states ψ_1, ψ_2 .

To study the jump of the boundary magnetization as shown in Fig. 3(c), we define the singular boundary magnetization:

$$m_{1s} = m_1(h_L) - m_{10}, \quad (60)$$

where m_{10} is the boundary magnetization at the transition point:

$$m_{10} = m_1(h_L)|_{h_L = -h_R}. \quad (61)$$

The transition point $h_L = -h_R$ is the midpoint of the jump as shown in Fig. 3(c). Since the scaling region in which the jump occurs approaches zero in the limit of $N \rightarrow \infty$, the variations in the extended state eigenvectors approach zero. Then the contribution from the extended states can be ignored so that the singular boundary magnetization is given by

$$m_{1s} \approx \frac{1}{2h_{L0}} (-\varepsilon_1 \psi_{1,0}^2 + \varepsilon_2 \psi_{2,0}^2) = \Delta_{m1} \frac{\kappa}{\sqrt{1 + \kappa^2}}, \quad (62)$$

where the boundary magnetization jump amplitude is given by $\Delta_{m1} = \varepsilon_R \alpha^2 / (2h_R^3)$. Figures 3(c) and 3(d) show the jump of the boundary magnetization and the FSS of the singular boundary magnetization. At the transition point $h_L = -h_R$, $\kappa = 0$, and then, we have $m_{1s} = 0$. From Eqs. (60) and (62), we can see that

$$m_{10} = \frac{1}{2h_{L0}} \sum_{k=3}^{N+1} \varepsilon_k \psi_{k,0}^2|_{h_L = -h_R}. \quad (63)$$

In particular, the boundary magnetization jump can be given exactly $h_R \rightarrow 0^-$. In this case, the above equation leads to

$$\lim_{h_R \rightarrow 0^-} \lim_{h_L \rightarrow -h_R + 0^+} \lim_{N \rightarrow \infty} m_1 = \sqrt{1 - g^2}. \quad (64)$$

Since $\sin \gamma_L = 0$ in Eq. (36) for $h_L \rightarrow 0$, $\psi_{k,0} = 0$ and the contribution to the boundary magnetization from all the extended states is zero. This boundary magnetization near the critical point $g < g_c = 1$ behaves as $m_1 \propto (g_c - g)^{\beta_1}$, where $\beta_1 = 1/2$. It has the same critical exponent of the boundary magnetization as the rectangular Ising model on a half-plane obtained by McCoy and Wu [17].

There should exist a first-order phase transition on a classical Ising strip with two surface fields as we change one surface field. To our knowledge, this has not been mentioned in previous work [19]. A possible reason is that those studies focused on the temperature-driven phase transition and ignored the boundary-field-driven phase transition. In the work by Campostrini *et al.* on the one-dimensional transverse field Ising model with boundary fields, the authors mentioned the wetting transition. However, in their setup, the boundary fields are perfectly asymmetric, so the interface is always at the middle of the chain, and the delocalization of the interface cannot be demonstrated explicitly [22].

V. THE CONTINUOUS WETTING TRANSITION

A. Connections between the classical wetting transition and the quantum wetting transition

Wetting phenomena have attracted enormous theoretical and experimental attention [27,28]. Such phenomena occur, e.g., in binary liquid mixtures below the consolute point, where one phase will generally be adsorbed on the wall of the container and may wet its surface at phase coexistence. The wetting transition can be viewed as a delocalization of the interface between the adsorbed phase and the bulk phase of the mixture. Far from the bulk critical temperature T_c , the interface is localized near the wall, but at some finite temperature less than T_c , the thickness of the wetting layer diverges. Due to the well-known correspondence between Ising ferromagnets and lattice-gas models of gas-fluid systems, the wetting transition can be studied using Ising models with surface fields [29]. In the ordered state, a continuous wetting transition is observed in the two-dimensional Ising model [20,21,30–32]. For an Ising ferromagnet with positive magnetization in the bulk, at zero bulk field, a negative boundary field H_1 at the wall may stabilize a domain with oppositely oriented magnetization at the surface.

Here we make some remarks on the classical wetting transition and its relation to the quantum transverse field Ising model. Classical wetting is the phenomenon in which a thick wetting layer of liquid is adsorbed at a planar wall-vapor interface. The wetting transition is described by three characteristic lengths: the thickness of the liquid x^* , the correlation length ξ_{\perp} for the fluctuation perpendicular to the wall and ξ_{\parallel} for the fluctuation parallel to the wall. The reduced temperature is defined by $t = 1 - T/T_w$, where T_w is the wetting transition temperature. The exponents related to x^* , ξ_{\perp} , ξ_{\parallel} are defined by $x^* \sim |t|^{-\beta_s}$, $\xi_{\perp} \sim |t|^{-\nu_{\perp}}$ and $\xi_{\parallel} \sim |t|^{-\nu_{\parallel}}$, respectively. For $d = 2$, the exact solution yields $\beta_s = 1$, $\nu_{\perp} = 1$, $\nu_{\parallel} = 2$ [20,21].

It is known that the one-dimensional quantum spin model can be mapped to the $1 + 1$ dimensional classical spin model [14]. The match of the wall in the classical model should be the left end of the spin chain in the quantum model. The

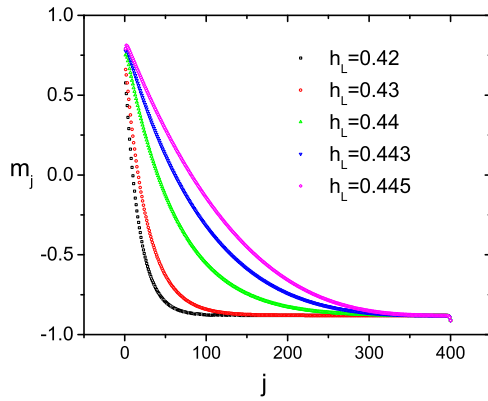


FIG. 4. Magnetization profiles for different h_L and $h_R = -1.0$, $g = 0.8$. The interface is delocalized as h_L approaches the wetting transition point $h_w = 0.4472 \dots$

parallel direction of the classical model should be the virtual time direction in the quantum model. The perpendicular direction in the classical model corresponds to the direction along the chain in the quantum model. There are one-to-one matches between the classical model and the quantum model.

The dynamical exponent is a basic critical exponent in the quantum phase transition. Here it corresponds to the correlation length exponent in the parallel direction in the classical model. The energy gap determines the dynamical exponent. According to the general theory of the quantum critical point, the energy gap vanishes as the z th power of the inverse correlation length [1]. In the Abraham model, $\nu_{\parallel} = 2\nu_{\perp}$ [20]. Therefore, we should have $\nu_{\parallel} = z\nu_{\perp}$. Since $\nu_{\parallel} = 2$, $\nu_{\perp} = 1$, $z = 2$. Below, our numerical results verify this conclusion.

The other critical exponents for the Abraham model is summarized in Table 1 of Ref. [32].

B. Rigorous proof of the second-order phase transition

The wetting transition occurs at

$$h_L = h_w = \sqrt{1-g} \quad (65)$$

for $h_R < -\sqrt{1-g}$. The other three cases for the wetting transition can be obtained by considering the symmetry.

Since the boundary fields have opposite signs, the magnetization profile has an interface, where the boundary magnetization changes sign. In Fig. 4 we show the magnetization profile for a chain with size $N = 400$ and $g = 0.8$, $h_R = -1$. The thickness of the positive magnetization layer becomes very large as h_L approaches $h_w = \sqrt{1-g} = 0.4472 \dots$ as shown in Fig. 4. In fact, this phase transition is the quantum version of the wetting transition on the Abraham model, which is an Ising strip with two surface fields [19,20]. We call this phase transition the quantum wetting transition. In the wetting phase shown in Fig. 1, the interface is delocalized and is located far away from the boundaries. In the ‘‘Positive’’ and ‘‘Negative’’ phases, the interface is localized at one boundary, so they can be called ‘‘Nonwet’’ phases.

In this wetting transition, a cusp in the boundary magnetization m_1 is present, as shown in Fig. 1(d). This cusp indicates that the derivative of m_1 with respect to h_L is discontinuous. We present some more detailed numerical results for

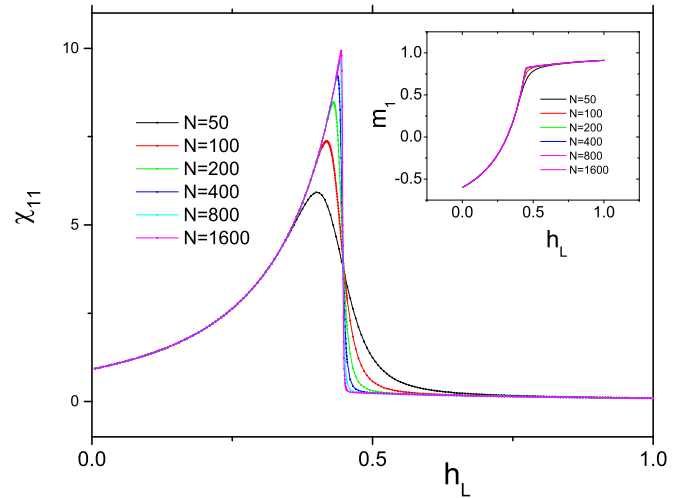


FIG. 5. Boundary susceptibility and magnetization (inset) for different sizes and $g = 0.8$, $h_R = -1.0$.

the boundary magnetization and susceptibility for finite-size lattices and $g = 0.8$, $h_R = -1$ in Fig. 5. In the numerical calculation, we compute the boundary magnetization m_1 with Eq. (27). Then, we use the difference method to calculate the boundary susceptibility:

$$\chi_{11} = \frac{\partial m_1}{\partial h_L} \approx \frac{m_1(h_L + \Delta h_L) - m_1(h_L - \Delta h_L)}{2\Delta h_L}. \quad (66)$$

In our calculation, we set $\Delta h_L = 10^{-7}$. In Fig. 5 the boundary susceptibility shows the typical features of a continuous phase transition. The boundary magnetization is continuous at the transition point (see the inset in Fig. 5), but χ_{11} makes a finite jump. This observation indicates that the critical index α_s linked to the boundary susceptibility $\chi_{11} \sim (h_w - h_L)^{-\alpha_s}$ is given by

$$\alpha_s = 0. \quad (67)$$

In the continuous wetting transition in the Abraham model [20], the boundary susceptibility has a jump. Our result shows that the quantum model is in perfect agreement with the Abraham model.

This singularity can be shown analytically. As discussed in Sec. III, a localized state eigenvector exists for $h_L < h_w < |h_R|$ and vanishes for $h_L > h_w$, which is described by Eq. (27). We denote the contribution from this localized state eigenvector ψ_1 to the boundary magnetization m_1 by I_1 . For $h_w - h_L \rightarrow 0$, in the limit $N \rightarrow \infty$, it is given by

$$I_1 = -\frac{1}{2h_L} \varepsilon_1 \psi_{1,0}^2 = -\frac{\varepsilon_L \alpha^2}{2h_L^3} = \frac{4}{g} (h_L - h_w), \quad (68)$$

where $\psi_{1,0}$ is the value of localized eigenvector at the site zero. For $h_L < h_w$, ψ_1 is a localized eigenvector, and ψ_1 becomes extended for $h_L > h_w$ so that we have $I_1 = 0$ for $h_L > h_w$. Hence, this term causes a jump $-4/g$ in χ_{11} . The contribution to m_1 from the extended states eigenvectors is given by

$$I_2 = \begin{cases} \frac{1}{2h_L} \sum_{n=2}^{N+1} \varepsilon_n \psi_{n,0}^2, & h_L < h_w \\ \frac{1}{2h_L} (-\varepsilon_1 \psi_{1,0}^2 + \sum_{n=2}^{N+1} \varepsilon_n \psi_{n,0}^2), & h_L > h_w \end{cases} \quad (69)$$

for $h_L > h_w$, where ψ_1 is the extended state with the lowest energy. The derivative of this quantity $\partial I_2/\partial h_L$ is also discontinuous at $h_L = h_w$. In the limit of $N \rightarrow \infty$, this becomes

$$I_2(h_L, a, b) = \int_0^\pi \frac{2\sqrt{1+g^2-2g\cos k}}{\pi h_L^3 [(a \tan(k/2) + b/\sin k)^2 + 1]} dk \quad (70)$$

for both cases $h_L < h_w$ and $h_L > h_w$. The parameters a, b are defined in Eq. (37). The singularity stems from the term $b/\sin k$. Near the wetting transition point, $b \approx 2h_w(h_L - h_w)/g$. We investigate the singular behavior of I around $|h_L - h_w| \ll 1$. To calculate $\partial I_2/\partial h_L$, we consider $I_2(h_w, a(h_w), b(h_L)) - I_2(h_w, a(h_w), b(h_w))$ in the limit $b \rightarrow 0$. The integrand is almost zero for $k \gg b$. The integration is contributed mainly from $k \sim b$. Therefore, we obtain

$$\begin{aligned} & \lim_{h_L \rightarrow h_w} I_2(h_w, a(h_w), b(h_L)) - I_2(h_w, a(h_w), b(h_w)) \\ &= \int_0^\infty \frac{2(1-g)dk}{\pi h_w^3} \left[\frac{1}{(b/k)^2 + 1} - 1 \right] = -\frac{|b|}{h_w}. \end{aligned} \quad (71)$$

Some calculations shows that this term causes a jump $-4/g$ in χ_{11} . Combining two parts I_1, I_2 from the localized state and extended states, we obtain the jump of the boundary susceptibility χ_{11} at the wetting transition point $h_L = h_w$ according to

$$\chi_{11}|_{h_L=h_w+0^+} - \chi_{11}|_{h_L=h_w-0^+} = -\frac{8}{g}. \quad (72)$$

In Fig. 5, $g = 0.8$, the jump of χ_{11} in the numerical result for $N = 1600$ is indeed close to -10 . It should be noted that for $h_L h_R > 0$, the singularities from the localized state and the extended states cancel so that there is no phase transition because the two boundary fields have the same sign.

C. Energy gap

For $h_L > h_w = \sqrt{1-g}$, the system is gapless. For $|h_L|, |h_R| > \sqrt{1-g}$, all the eigenvectors are extended states, and the energies are given by Eq. (34). It is clear that the gap $\Delta = \varepsilon_2 - \varepsilon_1 \rightarrow 0$ as the lattice size N approaches infinity.

For $h_L < h_w = \sqrt{1-g}$, the system is gapped. In the limit of $N \rightarrow \infty$, the ground state is localized at the right boundary with energy ε_R given in Eq. (51). The first excited state is the extended state with energy given by Eq. (34), with $k \rightarrow 0$. Then, we have $\varepsilon_2 = 2(1-g)$ and

$$\Delta = \varepsilon_2 - \varepsilon_1 = 2 \left[(1-g) - h_L \sqrt{1 - \frac{g^2}{1-h_L^2}} \right]. \quad (73)$$

Considering the critical regime $h_w - h_L \ll 1$, where $h_w = \sqrt{1-g}$, the gap behaves as

$$\Delta = \frac{4}{g}(h_w - h_L)^2 + O((h_w - h_L)^3) \quad (74)$$

for $h_w - h_L \ll 1$. Therefore, the critical exponent for the energy gap is given by

$$z\nu_\perp = 2, \quad (75)$$

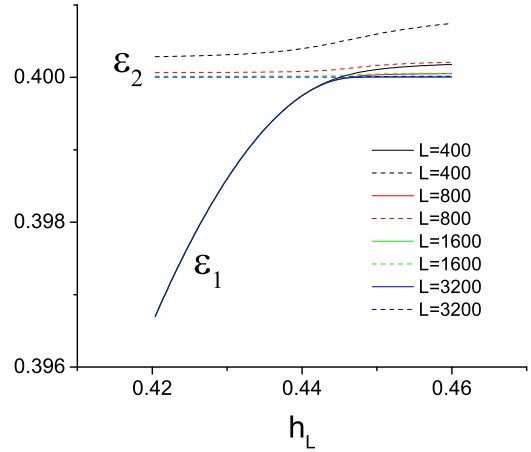


FIG. 6. Energies of the first excited state and the ground state for $g = 0.8$. The critical surface field is given by $h_w = \sqrt{1-g} = 0.44721\dots$

where ν_\perp is the correlation length exponent and z is the dynamical critical exponent that determines the relative rescaling factors of the space and time [1]. As mentioned above, the one-dimensional transverse field Ising model can be mapped to the two-dimensional Ising model. The transverse correlation in the two-dimensional Ising model should correspond to the correlation in the virtual time direction in the one-dimensional transverse field Ising model. The divergence of ξ_\parallel in the two-dimensional Ising model means that the gap vanishes in the one-dimensional transverse field Ising model. Later we will show that $\nu_\perp = 1$, such that we have $z = 2$, in agreement with the exact solution of the Abraham model, in which $\nu_\parallel = 2, \nu_\perp = 1$ [20,21].

We also verify the above conclusion on finite-size lattices numerically. We diagonalize the matrix \mathbf{C} using LAPACK. Such diagonalization can be carried out easily for lattice sizes up to $L = 3200$. Figure 6 shows the first and the second eigenvalues ε_1 and ε_2 for the lattice sizes $L = 400, 800, 1600, 3200$. For $L = 3200$, one can see that for $h_L < h_w = \sqrt{0.2} \approx 0.4472$, the energy gap opens, and for $h_L > h_w \approx 0.4472$, the gap closes.

In Fig. 7 we show the finite-size scaling of the gap Δ versus the scaling field $h_w - h_L$. The log-log plot shows that $\Delta \sim (h_w - h_L)^2$, in agreement with Eq. (74)

D. Magnetization profile, universal profile, and thickness of wetting layer

Similar to the boundary magnetization, we can calculate the magnetization at any site with Eq. (26). To compare our results with the field theory result for the two-dimensional Ising model with surface fields [32], we define

$$m(x) = m_j, \quad x = j, \quad (76)$$

where x is a continuous variable.

Figure 8(a) shows the magnetization profile away from the transition point and at the critical point for different lattice sizes. At the transition point $h_L = \sqrt{0.2}$, as shown in Fig. 8(b), the curves m versus x/L collapse for lattices from $L = 50$ to $L = 1600$. This result indicates the scale invariance at the

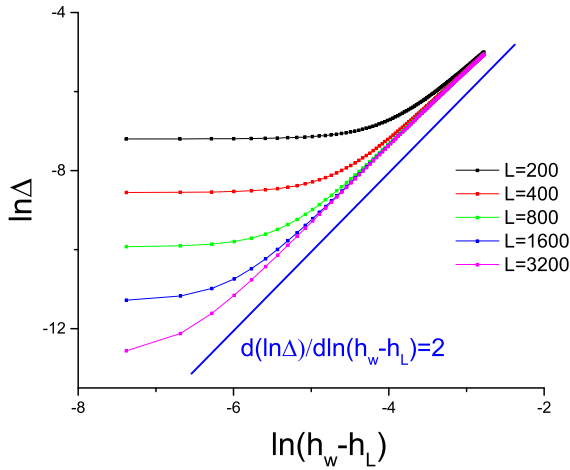


FIG. 7. Finite-size scaling of the energy gap.

critical point. By contrast, away from the critical point $h_L = 0.44$, the curves of m versus x/L do not collapse, as shown in Fig. 8(a).

To demonstrate the universality of the magnetization profiles at the different wetting transition points for different g , we also calculate the magnetization profile at the wetting transition point for $g = 0.36, 0.5, 0.64, 0.8$ for lattice size $L = 1600$. The wetting transition point is given by $h_L = \sqrt{1 - g}$. The curves m/m^* versus x/L collapse perfectly for the four situations.

Furthermore, we also obtain the analytical expression for the universal magnetization profile, even though we do not solve the model exactly. In Refs. [31,33], the magnetization profiles for a $d = 2$ Ising strip with opposite surface fields are studied. The universal magnetization profile is given by

$$\frac{m(x)}{m^*} = 1 - \frac{2x}{L} - \frac{2}{\pi} \sin\left(\frac{\pi x}{L}\right), \quad (77)$$

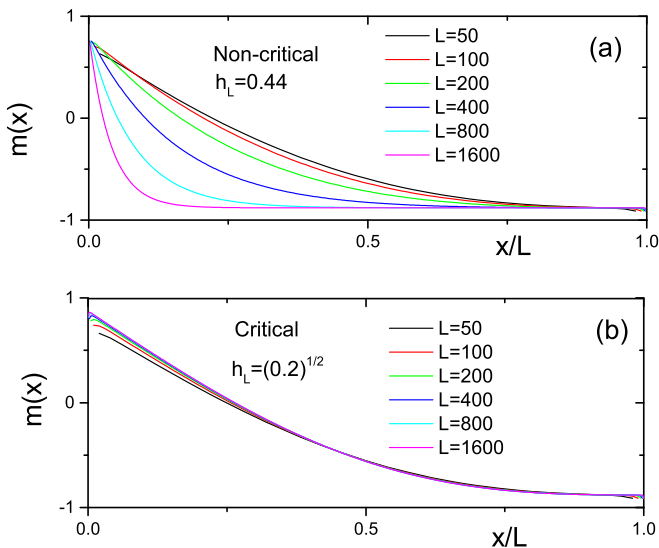
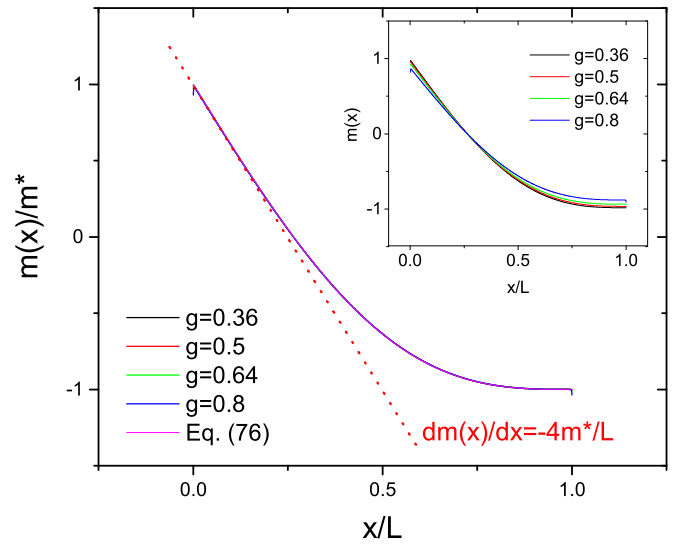


FIG. 8. Magnetization profile away from the transition point (a) and at the transition point (b).


 FIG. 9. Universality of the critical magnetization profile for different g . The exact result is given by Eq. (77). The inset shows the original curves of m versus x/L .

where m^* is the spontaneous magnetization in the bulk system. For the one-dimensional transverse field Ising model, it is given by [5]

$$m^* = (1 - g^2)^{1/8}. \quad (78)$$

As shown in Fig. 9, the magnetization profiles at the critical point for $g = 0.36, 0.5, 0.64, 0.8$ and the lattice size being $L = 1600$ collapse on the curve given by Eq. (77). The inset shows the original curves of m versus x/L . It should be emphasized that the above equation is not an analytical result for the one-dimensional transverse field Ising model but rather a result for the two-dimensional Ising model. Although we know that the two-dimensional Ising model can be mapped to the one-dimensional transverse field Ising model [14], this perfect collapse of the data and the perfect correspondence are still surprising. Moreover, we can conjecture that the above equation is precisely the rigorous result for the one-dimensional transverse field Ising model.

The thickness of the wetting layer is another diverging quantity at the transition point; in the present model, it is the number of sites where the magnetization is positive. From the magnetization profile, we can obtain the position x^* of the interface (or domain wall, where the magnetization is zero). x^* is the thickness. If $m_j > 0$ and $m_{j+1} < 0$, the magnetization changes sign, we obtain x^* by a simple interpolation

$$x^* = j + \frac{m_j}{m_j - m_{j+1}}. \quad (79)$$

It diverges near the wetting transition point as

$$x^* \sim (h_w - h_L)^{-\beta_s}. \quad (80)$$

Figure 10 shows the divergences of the thickness x^* and their finite-size scaling. From the figure, we observe that

$$\beta_s = 1. \quad (81)$$

This exponent is the same as that in the Abraham model [20,32].

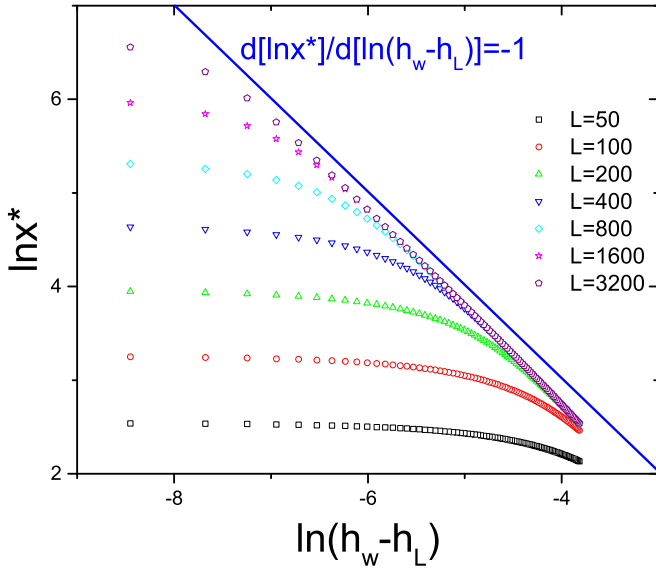


FIG. 10. Thickness of the wetting layer for a lattice size from $L = 50$ to $L = 3200$ and $g = 0.8$.

E. Correlation function and correlation length

The classical wetting transition in the Abraham model is anisotropic [20,21]. The correlation lengths along the directions parallel and perpendicular to the surface are different. Mapping to the one-dimensional transverse field Ising model, the parallel direction is the virtual time direction. The perpendicular direction is the direction along the Ising chain direction.

We can calculate the correlation function along the chain direction with Eq. (25). For simplicity, we calculate $c_{1,j}$:

$$c_{1,j} = \langle \Psi_1 | \sigma_1^{(1)} \sigma_j^{(1)} | \Psi_1 \rangle - m_1 m_j, \quad (82)$$

where m_1, m_j are the magnetization at sites 1, j , given by Eq. (26). Since the magnetization on each site is not zero, it is necessary to subtract the product of the magnetization at the two sites. Some examples of the correlation function are shown in Fig. 11, which is plotted in semilog scale. For $h_L = 0.48, 0.5, 0.6$, where the system is in the wetting phase, the correlation of other spin with the first left decays rapidly to become negligible. For $h_L < 0.447$, where the system is at the nonwet phase, the correlation decays with distance from the first spin exponentially, i.e., $c_{1,j} \sim e^{-(j-1)/\xi}$. Then, we can define the correlation length at this regime. We choose two spins at sites j_1 and j_2 and calculate the correlation length with

$$\xi = (j_2 - j_1) / \ln(c_{1,j_1}/c_{1,j_2}). \quad (83)$$

In the numerical calculation, we set $j_1 = 50, j_2 = 100$. Figure 12 shows the divergence of the correlation length near the wetting transition point. It should diverge at the wetting transition point as

$$\xi \sim (h_w - h_L)^{-\nu_\perp}. \quad (84)$$

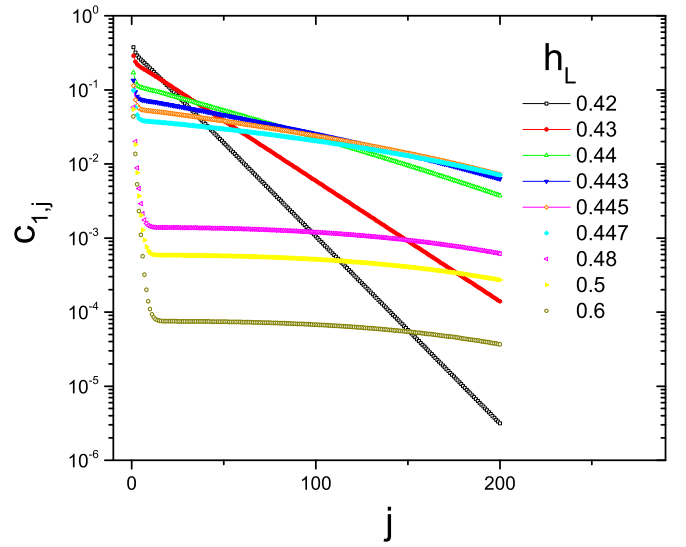


FIG. 11. Correlation functions near the left end. These correlation functions are obtained on the lattice with $L = 400, g = 0.8$.

From Fig. 8 we observe that the critical exponent should be

$$\nu_\perp = 1. \quad (85)$$

This exponent is also the same as that in the classical Abraham model [20,32].

VI. SUMMARY

In summary, we present the diagram of the one-dimensional transverse field Ising model with boundary fields. The exact FSS of the boundary magnetization in the first-order phase transition is obtained. The singularity of the boundary magnetization in the second-order quantum wetting transition is explicitly shown. Tuning the boundary fields should be simple in the experimental realization. Our work may be tested in future experiments with cold atoms [4].

We also proposed a computational procedure to numerically study the one-dimensional transverse field Ising model with boundary fields. The computational procedure provides

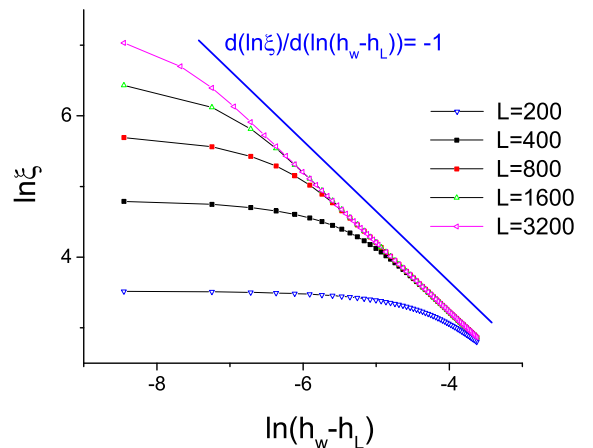


FIG. 12. Correlation length near the wetting transition point for the lattices with different sizes $L = 200, 400, 800, 1600, g = 0.8$.

an numerical method that is different from DMRG [22]. Our computational procedure can be carried out for $L = 3200$. To show the efficiency of this computational procedure, we compare it to the algorithm for the study of the wetting transition in the two-dimensional Ising model [34]. In that computational procedure, the the maximum of the transverse size is less than 400. The length of the Ising chain in our computational procedure can be 3200, or even larger. Moreover, this computational procedure can be extended to study the

model with disorder, for which it is very difficult to obtain the exact solution.

ACKNOWLEDGMENTS

The authors thank Prof. Wenan Guo and the SGI in the Department of Physics, Beijing Normal University, for providing computing time.

-
- [1] S. Sachdev, *Quantum Phase Transitions* (Cambridge University Press, Cambridge, 1999).
 - [2] M. Vojta, *Rep. Prog. Phys.* **66**, 2069 (2003).
 - [3] C. K. Chiu, J. C. Y. Teo, A. P. Schnyder, and S. Ryu, *Rev. Mod. Phys.* **88**, 035005 (2016)
 - [4] R. Islam, E. E. Edwards, K. Kim, S. E. Korenblit, C. Noh, H. J. Carmichael, G. D. Lin, L. M. Duan, C. C. J. Wang, J. K. Freericks *et al.*, *Nat. Commun.* **2**, 377 (2011).
 - [5] P. Pfeuty, *Ann. Phys.* **57**, 79 (1970).
 - [6] M. Campostrini, J. Nespolo, A. Pelissetto, and E. Vicari, *Phys. Rev. Lett.* **113**, 070402 (2014).
 - [7] M. Campostrini, A. Pelissetto, and E. Vicari, *Phys. Rev. B* **89**, 094516 (2014).
 - [8] A. Pelissetto, D. Rossini, and E. Vicari, *Phys. Rev. E* **98**, 032124 (2018).
 - [9] M. Campostrini, A. Pelissetto, and E. Vicari, *Phys. Rev. E* **91**, 042123 (2015).
 - [10] A. Pelissetto, D. Rossini, and E. Vicari, *Phys. Rev. E* **102**, 012143 (2020)
 - [11] H. T. Quan, Z. Song, X. F. Liu, P. Zanardi, and C. P. Sun, *Phys. Rev. Lett.* **96**, 140604 (2006).
 - [12] A. Kitaev, *Ann. Phys. (NY)* **321**, 2 (2006).
 - [13] X. Y. Feng, G.-M. Zhang, and T. Xiang, *Phys. Rev. Lett.* **98**, 087204 (2007).
 - [14] M. Suzuki, *Prog. Theor. Phys.* **56**, 1454 (1976).
 - [15] L. Onsager, *Phys. Rev.* **65**, 117 (1944).
 - [16] C. N. Yang, *Phys. Rev.* **85**, 808 (1952).
 - [17] R. M. McCoy and T. T. Wu, *Phys. Rev.* **162**, 436 (1967).
 - [18] H. Au-Yang and M. E. Fisher, *Phys. Rev. B* **21**, 3956 (1980).
 - [19] A. Maciolek and J. Stecki, *Phys. Rev. B* **54**, 1128 (1996).
 - [20] D. B. Abraham, *Phys. Rev. Lett.* **44**, 1165 (1980).
 - [21] D. B. Abraham, in *Phase Transition and Critical Phenomena*, edited by C. Domb and J. L. Lebowitz (Academic, London, 1986), Vol. 10, p. 1.
 - [22] M. Campostrini, A. Pelissetto, and E. Vicari, *J. Stat. Mech.: Theory Exp.* (2015) P11015.
 - [23] R. Z. Bariev and I. Peschel, *Phys. Lett. A* **153**, 166 (1991).
 - [24] H. Hinrichsen, K. Krebs, and I. Peschel, *Z. Phys. B* **100**, 105 (1996).
 - [25] U. Bilstein and B. Wehefritz, *J. Phys. A: Math. Gen.* **32**, 191 (1999).
 - [26] E. Lieb, T. Schultz, and D. Mattis, *Ann. Phys.* **16**, 407 (1961).
 - [27] P. G. de Gennes, *Rev. Mod. Phys.* **57**, 827 (1985).
 - [28] D. Bonn, J. Eggers, J. O. Indekeu, J. Meunier, and E. Rolley, *Rev. Mod. Phys.* **81**, 739 (2009).
 - [29] K. Binder and D. P. Landau, *Phys. Rev. B* **37**, 1745 (1988).
 - [30] E. V. Albano and K. Binder, *Phys. Rev. Lett.* **109**, 036101 (2012)
 - [31] A. O. Parry, *J. Phys. A: Math. Gen.* **24**, 1335 (1991).
 - [32] A. O. Parry, *J. Phys. A: Math. Gen.* **25**, 257 (1992).
 - [33] A. Maciolek, *J. Phys. A: Math. Gen.* **29**, 3837 (1996).
 - [34] X. Wu, *J. Stat. Phys.* **157**, 1284 (2014).